# Liquid and Glass Phases of an Alkylguanidinium Sulfonate Hydrogen-Bonded Organic Framework

Adam H. Slavney, Hong Ki Kim, Songsheng Tao, Mengtan Liu, Simon J. L. Billinge, and Jarad A. Mason*

ACCESS |    Metrics & More   |   Article Recommendations   |   Supporting Information

**ABSTRACT:** Glassy phases of framework materials feature unique and tunable properties that are advantageous for gas separation membranes, solid electrolytes, and phase-change memory applications. Here, we report a new guanidinium organosulfonate hydrogen-bonded organic framework (HOF) that melts and vitrifies below 100 °C. In this low-temperature regime, non-covalent interactions between guest molecules and the porous framework become a dominant contributor to the overall stability of the structure, resulting in guest-dependent melting, glass, and recrystallization transitions. Through simulations and X-ray scattering, we show that the local structures of the amorphous liquid and glass phases resemble those of the parent crystalline framework.

Liquid and glass phases of framework materials offer new opportunities for controlling the local structure and free volume of fluid and disordered states of matter through the application of reticular design principles.[1] However, liquid phases of many frameworks—and the melt-quenched glasses that can be derived from them—are difficult to access because melting temperatures often exceed framework decomposition temperatures. In metal−organic frameworks (MOFs), melting transitions can be made accessible by increasing the decomposition temperature through the selection of organic ligands with high thermal stability[1b,2] or by decreasing the melting temperature through the formation of weak metal−ligand coordination bonds.[3] While both of these strategies can lead to MOF liquids and glasses, they have, at least to date, offered fairly limited structural and chemical diversity.

Similar to metal−ligand coordination bonds in MOFs, directional interactions between hydrogen-bond donors and acceptors can be leveraged to form two- and three-dimensional hydrogen-bonded organic frameworks (HOFs) with predictable extended structures and tunable pore sizes and shapes.[4] Since the energy required to break hydrogen bonds—generally 15 to 65 kJ/mol[5]—is much less than that for metal−ligand coordination bonds (>300 kJ/mol for a typical Zn−carboxylate bond),[1d] HOFs offer a potential platform for framework materials with lower-temperature, more accessible melting transitions. Though glass formation has been studied for small molecules with intermolecular hydrogen bonds,[6] the melting and glass formation behavior of HOFs is relatively unexplored, particularly in comparison with that of MOFs. Here we demonstrate that a desymmetrization strategy can provide access to HOFs with low melting temperatures and HOF glasses with local structures that resemble their parent framework. Moreover, we highlight the important role of physisorbed guests in the melting and recrystallization behavior of these frameworks.

Most HOFs reported to date were designed to maximize framework stability, with hydrogen-bond donors and acceptors engaged in a large number of strong hydrogen bonds in high-symmetry structures.[4a,7] Though most HOFs thermally decompose prior to melting—similar to MOFs—the large family of guanidinium organosulfonate HOFs provide a notable exception and have reported melting temperatures at or above 200 °C (Table S1).[8] In these compounds, guanidinium cations form layered, hexagonal hydrogen-bonded networks with rigid bis(sulfonate) anions, creating solvent-filled channels between the hydrogen-bonded layers.[9] While guanidinium bis(sulfonates) have been known since the 1990s,[10] accessible microporosity, stability toward guest removal, and reversible melting transitions have only recently been demonstrated.[8] Long-chain alkyl monosulfonates paired with guanidinium also show melting transitions above 175 °C and undergo liquid-crystal transitions at lower temperatures.[11] However, these compounds form dense, interdigitated bilayers between the hydrogen-bonded sheets rather than a framework structure.

Though select guanidinium sulfonates are known to melt at lower temperatures than many meltable MOFs, much remains to be understood about the structural and chemical factors that influence the thermodynamics of HOF melting transitions. Following an approach pioneered for the design of ionic liquids,[12] we hypothesized that lowering the symmetry of the $D_{3h}$-symmetric guanidinium cation would provide a greater thermodynamic driving force for melting by increasing the rotational entropy of the liquid.[13] In particular, substituting N-methylguanidinium (MeG) for guanidinium (G) decreases the cation symmetry to $C_s$ but should still preserve the same layered hydrogen-bonding network, as previously shown for monosulfonates.[14]

To ensure the formation of solvent-accessible internal surfaces, we selected the rigid anion phenyl ether disulfonate (PEDS) for pairing with MeG. The guanidinium version of this compound, $(G)_2(PEDS)$, is known and adopts the characteristic hydrogen-bonded layer structure of guanidinium bis-(sulfonates).[15] We synthesized $(MeG)_2(PEDS)$ from (MeG)Cl and Ca(PEDS) via an ion exchange strategy (see the Supporting Information for details).

The structures of crystalline $(MeG)_2(PEDS)$ with different guest molecules were determined by single-crystal X-ray diffraction. Overall, $(MeG)_2(PEDS)$ adopts a structure similar to that of $(G)_2(PEDS)$ (Figure 1) with a similar hydrogen-
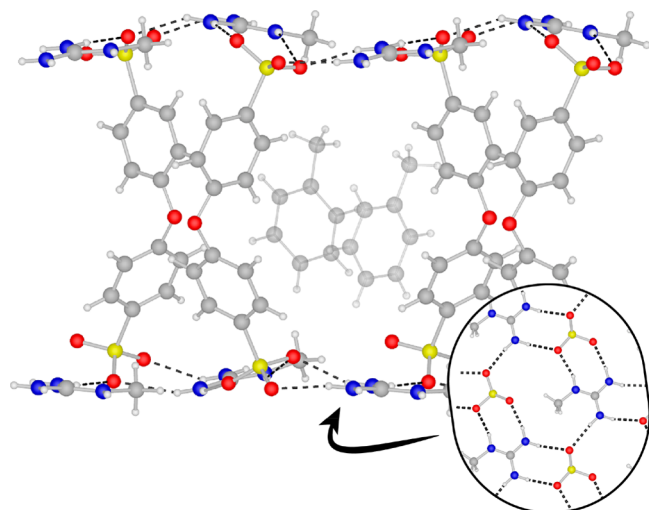


**Figure 1.** Crystal structure of $(MeG)_2(PEDS) \cdot$ toluene. Yellow, gray, blue, red, and white spheres represent S, C, N, O, and H atoms, respectively. The inset shows the hydrogen-bonding network in $(MeG)_2(PEDS)$.

bonding network, even though some MeG cations form only five hydrogen bonds (Figure 1, inset and Figure S1). As with other HOFs, different organic guests give crystals with slightly different unit cell dimensions and space groups (see Table S3) but the same overall connectivity.

To evaluate the impact of exchanging G for MeG on the melting behavior, we determined the melting temperatures for both $(G)_2(PEDS) \cdot$ toluene—the thermal properties of which have not been previously evaluated—and $(MeG)_2(PEDS) \cdot$ toluene by differential scanning calorimetry (DSC). Our initial experiments on $(MeG)_2(PEDS) \cdot$ toluene showed that partial guest desorption occurred to different degrees depending on the measurement conditions, masking the true melting temperature of each compound. To address this, we created a saturated toluene atmosphere above the sample by adding a small amount of liquid toluene to the pan, which was sealed with a lid pierced by a 70 $\mu$m pinhole—a standard method for DSC measurements on volatile samples. Thermogravimetric analysis (TGA) showed that these modifications prevented low-temperature guest desorption: above the normal toluene boiling point, the sample composition approached the expected 1:1 HOF-to-toluene molar ratio, consistent with the presence of the stochiometric compounds under these conditions (Figure 2A). For $(G)_2(PEDS) \cdot$ toluene, we observed two well-separated thermal events via DSC. The first, emerging gradually at 140 °C, was confirmed by TGA to correspond to desorption of toluene and was followed by melting of the guest-free framework at 202 °C. In contrast, for $(MeG)_2(PEDS) \cdot$ toluene the guest desorption and framework melting events overlapped, producing a combined peak with an onset of 126 °C. Melting points of both compounds were confirmed visually in glass capillaries (Figure S3).

As anticipated, the melting point of $(MeG)_2(PEDS)$ is significantly lower than that of $(G)_2(PEDS)$. Remarkably, the combined melting and desorption endotherm in $(MeG)_2(PEDS)$ occurs 14 °C lower than the onset of toluene desorption in $(G)_2(PEDS)$, even though the non-covalent interactions between toluene and the framework should be similar in the two structures. This suggests that framework melting may trigger the rapid vaporization of toluene guest molecules for $(MeG)_2(PEDS)$. Though the overlap of melting and desorption processes in $(MeG)_2(PEDS)$ precludes the rigorous determination of melting thermodynamics, it is clear that the lower-symmetry MeG cation leads to a substantial reduction in melting temperature.
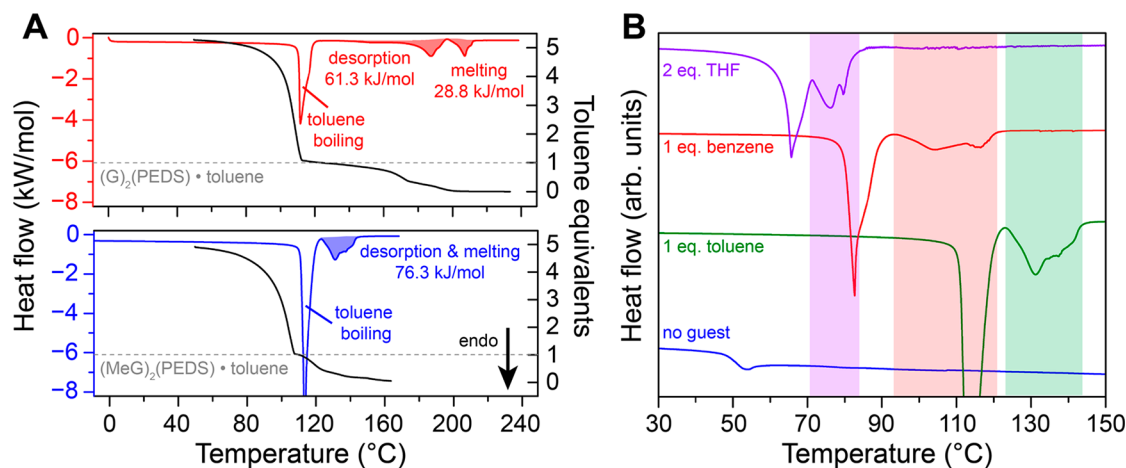


**Figure 2.** (A) Combined DSC and TGA traces of (top) $(G)_2(PEDS) \cdot$ toluene and (bottom) $(MeG)_2(PEDS) \cdot$ toluene. (B) Comparison of DSC traces of $(MeG)_2(PEDS)$ with different guest molecules. Melting and desorption regions are indicated by colored vertical bars. Without a guest, only a glass transition is observed. Melting is preceded by boiling of excess solvent, which is present to prevent low-temperature desorption of guests.

Given the interconnection between melting and guest desorption in $(MeG)_2(PEDS)$, we anticipated that host–guest interactions would have a strong influence on the melting behavior. Indeed, the melting behavior of $(MeG)_2(PEDS)$ varies widely depending on the identity of the guest present in the pores and scales with the strength of interactions between the guest and framework (Figure 2B). More weakly bound guests like THF show melting temperatures as low as 72 °C. Overall, the manipulation of the identity and occupation of guests within framework materials may be a general strategy to influence their melting transitions.[16]

Regardless of the identity of guest molecules that were originally present, $(MeG)_2(PEDS)$ loses crystallinity upon complete or partial desolvation (Figures 3 and S5) and forms
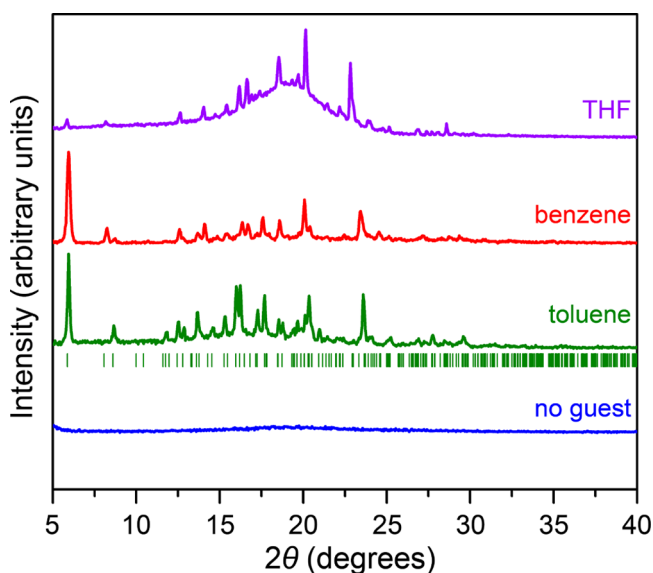


**Figure 3.** Powder X-ray diffraction patterns of a sample of glassy $(MeG)_2(PEDS)$ (blue) before and after it was melted and stirred with various organic solvents. Green tick marks correspond to the calculated Bragg peaks for the $(MeG)_2(PEDS)$·toluene. The hump in the THF background is from diffuse scattering of excess liquid THF, which prevents rapid hydration of the sample.

an ionic liquid above—or glass below—its glass transition temperature of 49 °C. To the best of our knowledge, this is the first example of a protic bis(sulfonate) ionic liquid, though the liquid is relatively viscous below 100 °C ($9.0 \times 10^5$ mPa·s at 90 °C; Figure S6) and has a fragility index of 60 (Figure S7). We note that the observed low glass transition temperature and high fluidity compared with liquids of zeolitic imidazolate frameworks (ZIFs), which reach similar viscosities only above 600 °C,[2,17] can be attributed to the reduced strength of hydrogen bonds relative to metal−ligand coordination bonds. The guest-free glass is highly stable, and we have not observed crystallization over the course of several days regardless of thermal treatment. However, contacting $(MeG)_2(PEDS)$—in either ionic liquid or glass form—with THF, benzene, or toluene slowly converts the material back to a crystalline framework via a surface reaction at the interface of the immiscible organic and ionic liquids (Figures 3 and S8−S10). Together, these observations suggest that the adsorption and desorption of guest molecules is intrinsically coupled to the crystallization and melting behavior of $(MeG)_2(PEDS)$. While many HOFs are known to collapse to form amorphous powders when guests are removed,[4b] to the best of our knowledge, this is the first demonstration of a HOF that transitions directly to an ionic liquid upon guest removal.

To gain insight into the local structure of liquid and glassy $(MeG)_2(PEDS)$, we performed density functional theory-based tight-binding molecular dynamics (DFTB-MD) simulations starting from the crystal structure of $(MeG)_2(PEDS)$·toluene with the toluene removed. At 45 °C, we observed rapid collapse of the framework to a denser phase (Supporting Video 1 and Figure S11). The collapsed structure is consistent with the lack of accessible porosity in glassy $(MeG)_2(PEDS)$, as determined by $N_2$ porosimetry (Figure S13).

The MD simulation indicated that despite the pore collapse, the layered structure of the framework persists to some degree in the amorphous phase (Figure 4A). Additionally, the hydrogen bonding of the framework is maintained: the average number of hydrogen bonds increases in the ionic liquid (from 5.5 to 5.6 hydrogen bonds per MeG), albeit with a wider distribution of donor−acceptor distances (Figure S14). This is consistent with experimental infrared spectra that show no
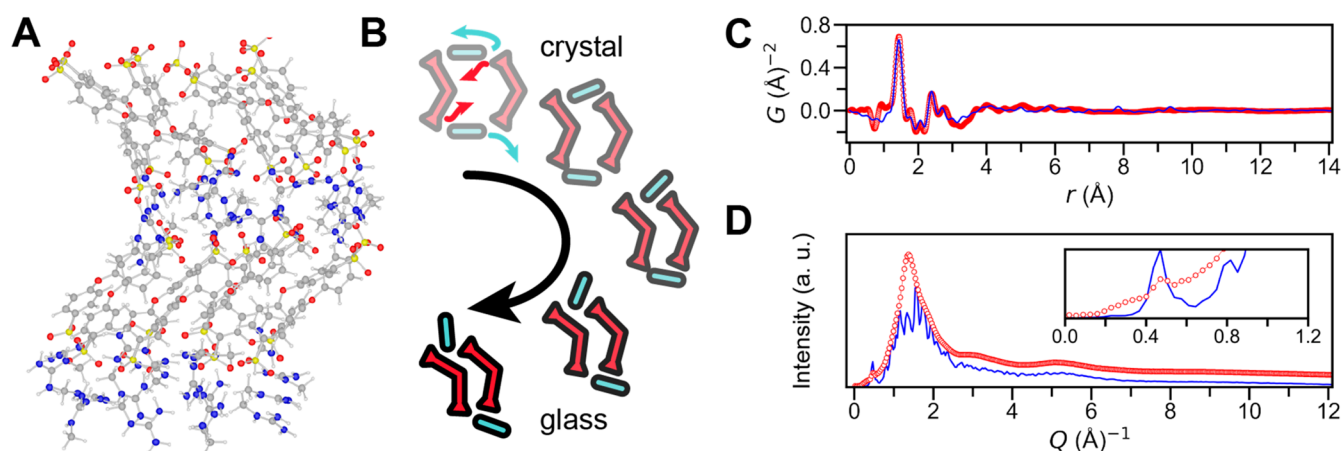


**Figure 4.** (A) Snapshot of the simulated amorphous phase of $(MeG)_2(PEDS)$, showing preservation of the layered structure. Yellow, gray, blue, red, and white sphere represent S, C, N, O, and H atoms, respectively. (B) Schematic showing an approximate mechanism of pore collapse and amorphization in $(MeG)_2(PEDS)$ due to reorientation of the MeG cations. (C) Pair distribution function and (D) X-ray total scattering pattern of amorphous $(MeG)_2(PEDS)$ at room temperature (red) compared with that calculated from MD simulations (blue). The inset in (D) shows the $Q$ = 0.47 peak due to a remnant layered structure.

C

differences in the N−H stretching region for the crystal and glass or liquid states (Figure S15).

The primary difference between the simulated amorphous structure and the crystalline framework lies in the orientation of the MeG cations relative to the sulfonate layers. In the crystalline state, the MeG cations lie flat, forming a bilayer structure, while in the amorphous state roughly half of the cations rotate by 90° to bridge between adjacent sulfonate layers. This reorientation drives pore collapse, as the sulfonate sublattice shrinks to maintain hydrogen bonding with the rotated MeG cations (Figure 4B). Similar differences in guanidinium cation orientation between the porous and nonporous crystalline phases of $(G)_2(1,4\text{-benzenedisulfonate})$ were observed.[8b]

We further validated our simulation results by obtaining the X-ray total scattering pattern and the pair distribution function (PDF) of amorphous $(MeG)_2(PEDS)$ and comparing them to simulated data based on the MD model (Figure 4C,D).[18,19] Below 7 Å, the experimental PDF shows sharp features, suggesting that the glass may be ordered at short distances. However, because this region is dominated by intramolecular scattering of the molecular components, additional techniques are needed to verify this. In ZIF glasses, similar sharp intramolecular features are observed in the PDF,[20] although solid-state NMR spectroscopy indicates short-range disorder in the glass.[21]

Beyond 7 Å, the experimental PDF contains a broad density modulation, indicating a lack of well-defined intermolecular distances and medium-range disorder. However, the total X-ray scattering data indicate that longer-range correlations are present. Specifically, there is an intense peak at $Q = 1.37$ Å$^{-1}$ ($d = 4.58$ Å) and an additional weak peak at $Q = 0.47$ Å$^{-1}$ ($d = 13.37$ Å) (Figure 4D inset). From the MD results, we can assign the intense peak to nearest-neighbor diffuse scattering. More remarkably, the weaker peak at $Q = 0.47$ Å$^{-1}$ is reproduced in the simulated pattern and can be traced to interlayer scattering, providing conformation of the layered amorphous structure predicted by DFTB-MD. It should be noted that the sharp peaks observed in the simulated scattering and PDF data can be attributed to the finite size of the MD simulation box, which is unable to capture the full range of orientations present in an amorphous sample.

The foregoing results demonstrate that a desymmeterization strategy can be used to design HOFs with melting points below 100 °C, accessible glass transitions, and interesting guest-dependent phase behavior. Additionally, we have shown that the local structure of the $(MeG)_2(PEDS)$ ionic liquid and glass retain many features inherited from the crystalline state. This creates exciting possibilities for the rational design of HOF glasses with tunable properties optimized for gas-separation membranes, phase-change memory applications, and—unique to HOFs—proton-conducting solid electrolytes.

## ■ ASSOCIATED CONTENT

### ⓢ Supporting Information

The Supporting Information is available free of charge at https://pubs.acs.org/doi/10.1021/jacs.2c02918.

> Additional experimental details, additional computational details, powder X-ray diffraction data, single-crystal X-ray diffraction data, NMR and IR spectra, and summaries of all structural and thermodynamic data (PDF)

MD simulation results (MP4)

### Accession Codes

CCDC 2159485, 2159498, and 2159711 contain the supplementary crystallographic data for this paper. These data can be obtained free of charge via www.ccdc.cam.ac.uk/data_request/cif, or by emailing data_request@ccdc.cam.ac.uk, or by contacting The Cambridge Crystallographic Data Centre, 12 Union Road, Cambridge CB2 1EZ, U.K.; fax: +44 1223 336033.

## ■ AUTHOR INFORMATION

### Corresponding Author

**Jarad A. Mason** − *Department of Chemistry and Chemical Biology, Harvard University, Cambridge, Massachusetts 02138, United States;* ⓞ orcid.org/0000-0003-0328-7775; Email: mason@chemistry.harvard.edu

### Authors

**Adam H. Slavney** − *Department of Chemistry and Chemical Biology, Harvard University, Cambridge, Massachusetts 02138, United States*

**Hong Ki Kim** − *Department of Chemistry and Chemical Biology, Harvard University, Cambridge, Massachusetts 02138, United States;* ⓞ orcid.org/0000-0002-6115-384X

**Songsheng Tao** − *Department of Applied Physics and Applied Mathematics, Columbia University, New York, New York 10027, United States*

**Mengtan Liu** − *Department of Chemistry and Chemical Biology, Harvard University, Cambridge, Massachusetts 02138, United States*

**Simon J. L. Billinge** − *Department of Applied Physics and Applied Mathematics, Columbia University, New York, New York 10027, United States; Condensed Matter Physics and Materials Science Department, Brookhaven National Laboratory, Upton, New York 11973, United States*

Complete contact information is available at:
https://pubs.acs.org/10.1021/jacs.2c02918

### Notes

The authors declare no competing financial interest.

## ■ REFERENCES

(1) (a) Umeyama, D.; Horike, S.; Inukai, M.; Itakura, T.; Kitagawa, S. Reversible Solid-to-Liquid Phase Transition of Coordination Polymer Crystals. *J. Am. Chem. Soc.* **2015**, *137*, 864. (b) Gaillac, R.; Pullumbi, P.; Beyer, K. A.; Chapman, K. W.; Keen, D. A.; Bennett, T. D.; Coudert, F.-X. Liquid metal−organic frameworks. *Nat. Mater.* **2017**, *16*, 1149. (c) Bennett, T. D.; Horike, S. Liquid, glass and amorphous solid states of coordination polymers and metal−organic frameworks. *Nat. Rev. Mater.* **2018**, *3*, 431. (d) Yaghi, O. M.; O'Keeffe, M.; Ockwig, N. W.; Chae, H. K.; Eddaoudi, M.; Kim, J. Reticular synthesis and the design of new materials. *Nature* **2003**, *423*,

705. (e) Kitagawa, S.; Kitaura, R.; Noro, S.-i. Functional Porous Coordination Polymers. *Angew. Chem., Int. Ed.* **2004**, *43*, 2334. (f) Férey, G. Hybrid porous solids: past, present, future. *Chem. Soc. Rev.* **2008**, *37*, 191. (g) Ma, N.; Horike, S. Metal−Organic Network-Forming Glasses. *Chem. Rev.* **2022**, *122*, 4163.

(2) Bennett, T. D.; Tan, J.-C.; Yue, Y.; Baxter, E.; Ducati, C.; Terrill, N. J.; Yeung, H. H. M.; Zhou, Z.; Chen, W.; Henke, S.; Cheetham, A. K.; Greaves, G. N. Hybrid glasses from strong and fragile metal-organic framework liquids. *Nat. Commun.* **2015**, *6*, 8079.

(3) (a) Nagarkar, S. S.; Kurasho, H.; Duong, N. T.; Nishiyama, Y.; Kitagawa, S.; Horike, S. Crystal melting and glass formation in copper thiocyanate based coordination polymers. *Chem. Commun.* **2019**, *55*, 5455. (b) Liu, M.; McGillicuddy, R. D.; Vuong, H.; Tao, S.; Slavney, A. H.; Gonzalez, M. I.; Billinge, S. J. L.; Mason, J. A. Network-Forming Liquids from Metal−Bis(acetamide) Frameworks with Low Melting Temperatures. *J. Am. Chem. Soc.* **2021**, *143*, 2801.

(4) (a) Lin, R.-B.; He, Y.; Li, P.; Wang, H.; Zhou, W.; Chen, B. Multifunctional porous hydrogen-bonded organic framework materials. *Chem. Soc. Rev.* **2019**, *48*, 1362. (b) Hisaki, I.; Xin, C.; Takahashi, K.; Nakamura, T. Designing Hydrogen-Bonded Organic Frameworks (HOFs) with Permanent Porosity. *Angew. Chem., Int. Ed.* **2019**, *58*, 11160. (c) Li, P.; Ryder, M. R.; Stoddart, J. F. Hydrogen-Bonded Organic Frameworks: A Rising Class of Porous Molecular Materials. *Acc. Mater. Res.* **2020**, *1*, 77.

(5) Jeffrey, G. A. *An Introduction to Hydrogen Bonding*; Oxford University Press, 1997.

(6) (a) Lebel, O.; Maris, T.; Perron, M.-È.; Demers, E.; Wuest, J. D. The Dark Side of Crystal Engineering: Creating Glasses from Small Symmetric Molecules that Form Multiple Hydrogen Bonds. *J. Am. Chem. Soc.* **2006**, *128*, 10372. (b) Chen, Y.; Zhang, W.; Yu, L. Hydrogen Bonding Slows Down Surface Diffusion of Molecular Glasses. *J. Phys. Chem. B* **2016**, *120*, 8007. (c) Laventure, A.; Gujral, A.; Lebel, O.; Pellerin, C.; Ediger, M. D. Influence of Hydrogen Bonding on the Kinetic Stability of Vapor-Deposited Glasses of Triazine Derivatives. *J. Phys. Chem. B* **2017**, *121*, 2350.

(7) Brunet, P.; Simard, M.; Wuest, J. D. Molecular Tectonics. Porous Hydrogen-Bonded Networks with Unprecedented Structural Integrity. *J. Am. Chem. Soc.* **1997**, *119*, 2737.

(8) (a) Karmakar, A.; Illathvalappil, R.; Anothumakkool, B.; Sen, A.; Samanta, P.; Desai, A. V.; Kurungot, S.; Ghosh, S. K. Hydrogen-Bonded Organic Frameworks (HOFs): A New Class of Porous Crystalline Proton-Conducting Materials. *Angew. Chem., Int. Ed.* **2016**, *55*, 10667. (b) Brekalo, I.; Deliz, D. E.; Barbour, L. J.; Ward, M. D.; Frišćić, T.; Holman, K. T. Microporosity of a Guanidinium Organodisulfonate Hydrogen-Bonded Framework. *Angew. Chem., Int. Ed.* **2020**, *59*, 1997.

(9) Adachi, T.; Ward, M. D. Versatile and Resilient Hydrogen-Bonded Host Frameworks. *Acc. Chem. Res.* **2016**, *49*, 2669.

(10) Russell, V. A; Etter, M. C.; Ward, M. D. Layered Materials by Molecular Design: Structural Enforcement by Hydrogen Bonding in Guanidinium Alkane- and Arenesulfonates. *J. Am. Chem. Soc.* **1994**, *116*, 1941.

(11) (a) Mathevet, F.; Masson, P.; Nicoud, J.-F.; Skoulios, A. Smectic Liquid Crystals from Supramolecular Guanidinium Alkyl-benzenesulfonates. *Chem. - Eur. J.* **2002**, *8*, 2248. (b) Mathevet, F.; Masson, P.; Nicoud, J.-F.; Skoulios, A. Smectic Liquid Crystals from Supramolecular Guanidinium Alkanesulfonates. *J. Am. Chem. Soc.* **2005**, *127*, 9053.

(12) Hallett, J. P.; Welton, T. Room-Temperature Ionic Liquids: Solvents for Synthesis and Catalysis. 2. *Chem. Rev.* **2011**, *111*, 3508.

(13) (a) Wei, J. Molecular Symmetry, Rotational Entropy, and Elevated Melting Points. *Ind. Eng. Chem. Res.* **1999**, *38*, 5019. (b) Dannenfelser, R.-M.; Yalkowsky, S. H. Estimation of Entropy of Melting from Molecular Structure: A Non-Group Contribution Method. *Ind. Eng. Chem. Res.* **1996**, *35*, 1483.

(14) Burke, N. J.; Burrows, A. D.; Mahon, M. F.; Warren, J. E. Structural manipulation through control of hydrogen bonding faces: the effects of cation substitution on the guanidinium sulfonate structure. *CrystEngComm* **2006**, *8*, 931.

(15) Holman, K. T.; Martin, S. M.; Parker, D. P.; Ward, M. D. The Generality of Architectural Isomerism in Designer Inclusion Frameworks. *J. Am. Chem. Soc.* **2001**, *123*, 4421.

(16) Nozari, V.; Calahoo, C.; Tuffnell, J. M.; Keen, D. A.; Bennett, T. D.; Wondraczek, L. Ionic liquid facilitated melting of the metal-organic framework ZIF-8. *Nat. Commun.* **2021**, *12*, 5703.

(17) Qiao, A.; Bennett, T. D.; Tao, H.; Krajnc, A.; Mali, G.; Doherty, C. M.; Thornton, A. W.; Mauro, J. C.; Greaves, G. N.; Yue, Y. A metal-organic framework with ultrahigh glass-forming ability. *Sci. Adv.* **2018**, *4*, No. eaao6827.

(18) Chupas, P. J.; Qiu, X.; Hanson, J. C.; Lee, P. L.; Grey, C. P.; Billinge, S. J. L. Rapid-acquisition pair distribution function (RA-PDF) analysis. *J. Appl. Crystallogr.* **2003**, *36*, 1342.

(19) (a) Juhás, P.; Davis, T.; Farrow, C. L.; Billinge, S. J. L. *PDFgetX3*: a rapid and highly automatable program for processing powder diffraction data into total scattering pair distribution functions. *J. Appl. Crystallogr.* **2013**, *46*, 560. (b) Yang, X.; Juhás, P.; Farrow, C. L.; Billinge, S. J. L. xPDFsuite: an end-to-end software solution for high throughput pair distribution function transformation, visualization and analysis. *arXiv (Condensed Matter.Materials Science)*, February 23, 2015, 1402.3163, ver. 3. https://arxiv.org/abs/1402.3163 (accessed 2022-06-01). (c) Juhas, P.; Farrow, C. L.; Yang, X.; Knox, K. R.; Billinge, S. J. L. Complex modeling: a strategy and software program for combining multiple information sources to solve ill posed structure and nanostructure inverse problems. *Acta Crystallogr., Sect. A* **2015**, *71*, 562.

(20) Zhang, J.; Longley, L.; Liu, H.; Ashling, C. W.; Chater, P. A.; Beyer, K. A.; Chapman, K. W.; Tao, H.; Keen, D. A.; Bennett, T. D.; Yue, Y. Structural evolution in a melt-quenched zeolitic imidazolate framework glass during heat-treatment. *Chem. Commun.* **2019**, *55*, 2521.

(21) Madsen, R. S. K.; Qiao, A.; Sen, J.; Hung, I.; Chen, K.; Gan, Z.; Sen, S.; Yue, Y. Ultrahigh-field $^{67}$Zn NMR reveals short-range disorder in zeolitic imidazolate framework glasses. *Science* **2020**, *367*, 1473.